

Symmetries in the time-averaged dynamics of networks: reducing unnecessary complexity through minimal network models

Abu Bakar Siddique¹, Louis M. Pecora², and Francesco Sorrentino¹

¹*Department of Mechanical Engineering, The University of New Mexico*

²*Code 6343, Naval Research Laboratory, Washington, D.C. 20375*

Complex networks are the subject of fundamental interest from the scientific community at large. Several metrics have been introduced to characterize the structure of these networks, such as the degree distribution, degree correlation, path length, clustering coefficient, centrality measures etc. Another important feature is the presence of network symmetries. In particular, the effect of these symmetries has been studied in the context of network synchronization, where they have been used to predict the emergence and stability of cluster synchronous states. Here we provide theoretical, numerical, and experimental evidence that network symmetries play a role in a substantially broader class of dynamical models on networks, including epidemics, game theory, communication, and coupled excitable systems. Namely, we see that in all these models, nodes that are related by a symmetry relation show the same time-averaged dynamical properties. This discovery leads us to propose reduction techniques for exact, yet minimal, simulation of complex networks dynamics, which we show are effective in order to optimize the use of computational resources, such as computation time and memory.

1 Outline

In recent years a large body of research has investigated the dynamics of complex networks, including percolation [33], epidemics [34, 35], synchronization [1, 32, 5, 49, 50, 51, 52, 2, 3, 12], evolutionary games [17, 36], and traffic dynamics [25, 4, 6, 7, 24, 8, 13, 15, 16]. These studies are relevant to better model, understand, design, and control networks in technological, biological, and social applications. Extensive research has shown that the topology of these networks (e.g. their degree distribution [27, 42], degree correlation [40, 41], community structure [39], etc.) plays a significant role in their dynamical time evolution [47].

Another important feature of the network topology is the presence of network symmetries, which so far have remained to some extent unexplored, with some exceptions [12, 48, 31, 30, 14]. These symmetries have been shown to be commonplace in many real networks [29], hence it becomes important to understand how they can affect the dynamics of the network. References [12, 48, 31, 30, 14] have focused on the role played by the network symmetries on the emergence of cluster synchronization. Here we consider several well known dynamical models on networks and try to illustrate the effects of the underlying network symmetries on the network dynamics. Our study indicates that network symmetries play a role in all the dynamical models considered and in particular: evolutionary games [17, 36], network traffic [25, 4, 6, 7, 24, 8, 13, 15, 16], and propagation of excitation among excitable systems [9, 18, 11]; and thus suggests the effects of the symmetries on the dynamics may be a rather general feature of complex networks. However, as we will see, the particular effect of the symmetries varies based on the particular type of dynamics considered.

Here, the topology of a network is described by the adjacency matrix $A = \{A_{ij}\}$, where $A_{ij} = A_{ji}$ is equal to 1 if node j and i affect each other and is equal to 0 otherwise. We define a network symmetry as a permutation of the network nodes that leaves the network structure unaltered. The symmetries of the network form a (mathematical) group \mathcal{G} . Each element of the group can be described by a permutation matrix Π that re-orders the nodes in a way that leaves the network structure unchanged (that is, each Π commutes with A , $\Pi A = A \Pi$). Though the set of symmetries (or automorphisms) of a network can be quite large, even for small networks, it can be computed from knowledge of the matrix A by using widely available discrete algebra routines. In fact, except for simple cases for which it may be possible to identify the symmetries by inspection, in general for an arbitrary network, the use of a software is required. In this study we used Sage [21], an open-source mathematical software. Once the symmetries are identified, the nodes of the network can be partitioned into M clusters by finding the orbits of the symmetry

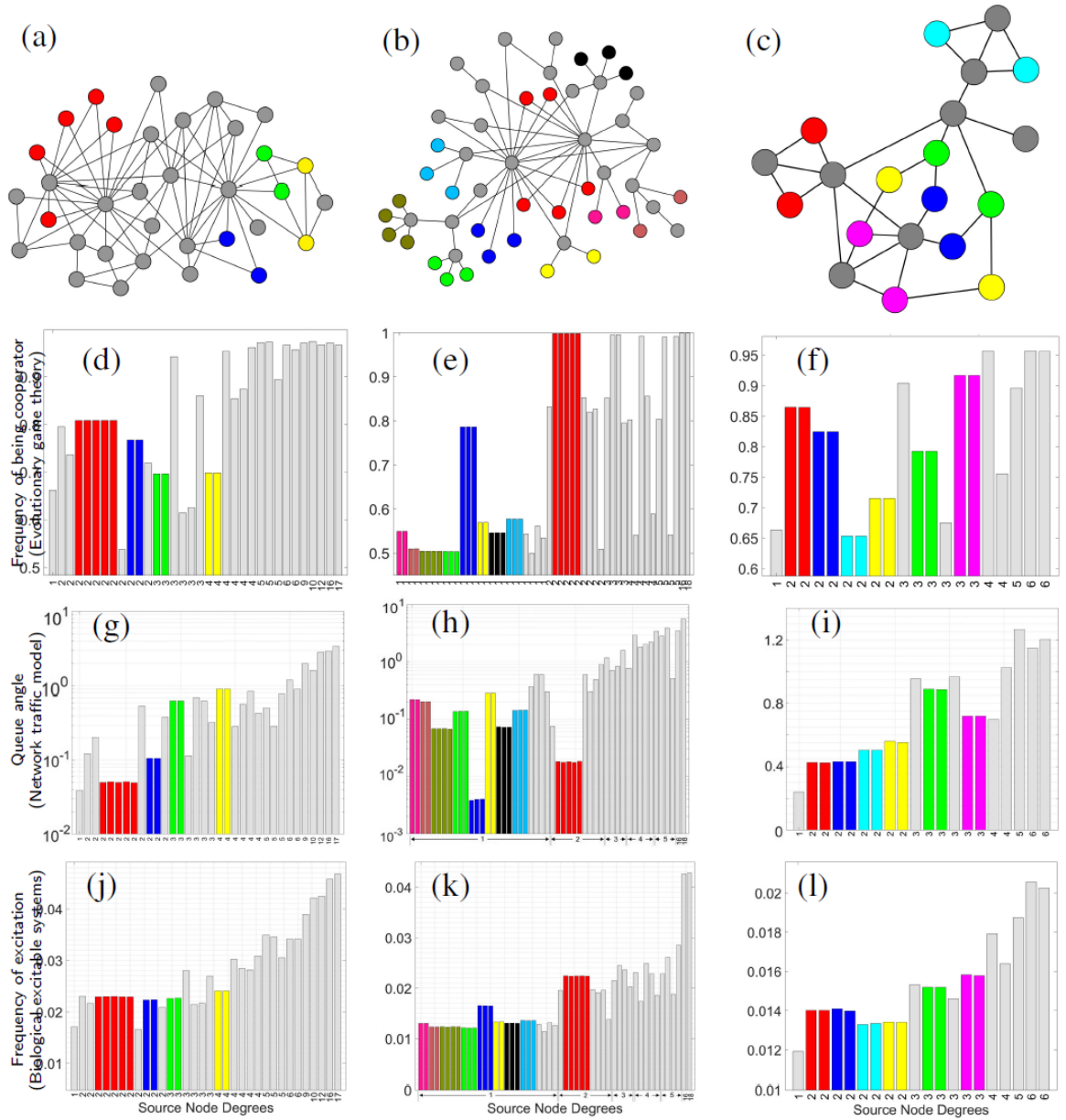


Figure 1: **Effects of the network symmetries in three different dynamical models/networks:** (a) the Zachary's Karate Club network [23], (b) the Bellsouth network [22] and (c) a random graph, nodes colored the same are in the same symmetry cluster except the gray colored nodes, each of which is in a cluster by itself. (d-f) Prisoner's Dilemma game played, (g-i) Network traffic model simulated and (j-l) dynamics of the Kinouchi Copelli model [9] in these networks (a-c).

group, i.e., the disjoint sets of nodes that, when all of the symmetry operations are applied, permute among one another in the same set.

2 Symmetries of the Network Dynamics

Figure 1(a), (b), and (c) shows three examples of undirected networks: the Zachary’s Karate Club network [23] of $N = 34$ nodes, the Bell South network [26] of $N = 51$ nodes and a randomly generated Erdős-Rényi (ER) graph of $N = 20$ nodes, respectively. Each node of the Karate Club network is a member of a university karate club and a connection represents a friendship relation between the members. The nodes of the Bell South network are the IP/MPLSs (Multiprotocol Label Switching: a switching mechanism used in high-performance telecommunications networks) backbone and connections represent routing paths. In Fig. 1(a), (b) and (c) colors of the nodes indicate the clusters they belong to, either non-trivial (i.e. clusters with more than one node in them) or trivial clusters (clusters with only one node in them). All the nodes in trivial clusters are colored gray, while the non-trivial clusters are colored differently. The Karate Club network in Fig. 1(a) has $C = 4$ nontrivial clusters, 23 trivial clusters and 480 symmetries. The Bell South network in Fig. 1(b) displays $C = 9$ nontrivial clusters, 24 trivial clusters and 29,859,840 symmetries. The random network in Fig. 1(c) has $C = 6$ non-trivial clusters, 8 trivial clusters and 8 symmetries. The rest of Fig. 1 has a total of nine panels, one for each of three networks and each of three dynamical models. The three dynamical models are: evolutionary game theory (d-f), network traffic (g-i), and propagation of excitation among excitable system (j-l). We now briefly introduce the models, which are all stochastic in nature.

2.1 Evolutionary Game Theory Model

The evolutionary game theory dynamics models the evolution of cooperation and defection in a population of coupled agents (nodes), playing the Prisoner’s Dilemma game. At each time step a node is randomly selected and its strategy is updated. The new strategy to be adopted is probabilistically determined based on the payoffs of the nodes surrounding the selected node and their strategy selection.

Each one of the network nodes (agents) iteratively plays a version of the Prisoner’s Dilemma game [17]. Each node i can either be a cooperater ($S_i = 1$) or a defector ($S_i = 0$). The network connectivity is defined by the adjacency matrix A , described earlier. We define a payoff between two players, based on the well known *Prisoner’s Dilemma* game. There are two types of strategy adopted by the players: *cooperation* and *defection*. A cooperater pays a cost c for each one of the agents it is connected to and a defector pays nothing [17]. Each node receives a benefit equal to b for each cooperater it is connected to. When playing the game, node i receives a payoff equal to

$$\xi_i = \sum_j (A_{ij}bS_j - A_{ji}cS_i). \quad (1)$$

We define the fitness [17] of each node to be $f_i = 1 - \omega + \omega\xi_i$, where $0 \leq \omega \leq 1$ measures the intensity of selection: $\omega \simeq 1$ means strong selection, that is the fitness is almost equal to the payoff and $\omega \simeq 0$ means weak selection, that is the fitness is almost independent of the payoff and close to 1. The literature [17, 44, 45, 43] focuses on the case of weak selection, which is also what we consider here (in all our simulations we either set $\omega = 0.1$ or $\omega = 0.2$). Following [17] we choose a ‘Death-birth’ (DB) updating rule for the game evolution. Namely, in each time step a randomly selected node i is replaced by a new offspring (node). The new offspring evolves into either a cooperater or a defector depending on the fitness of the surrounding agents. We set the probability of that new node to be a cooperater to be $\sigma(F_{Ci} - F_{Di})$, where F_{Ci} and F_{Di} are the fitnesses of cooperaters and defectors in the neighboring nodes and σ is a monotonically increasing function such that $0 \leq \sigma \leq 1$. This reflects a higher propensity of turning into a cooperater based on how *well* the neighbors of a given node that are cooperaters are doing with respect to the other neighbors of that node that are defectors. The total fitness of the neighbors of player i is equal to

$$F_i = \sum_j^N A_{ij}f_j \quad (2)$$

The total fitness of the cooperators, F_{Ci} and defectors, F_{Di} in the neighboring nodes of i is defined as,

$$\begin{aligned} F_{Ci} &= \sum_j^N A_{ij} S_j f_j = \sum_j^N A_{ij} S_j (1 - \omega) + \omega \sum_j^N A_{ij} S_j \xi_j \\ F_{Di} &= F_i - F_{Ci} = \sum_j^N A_{ij} (1 - S_j) (1 - \omega) + \omega \sum_j^N A_{ij} (1 - S_j) \xi_j \end{aligned} \quad (3)$$

Letting $x_i = (F_{Ci} - F_{Di})$, we write the probability that the new offspring will be a cooperator $\sigma(x_i)$. Here we set $\sigma(x_i) = \gamma x_i + \varepsilon$, where $\gamma > 0$ and ε are two arbitrary constants. In all our numerical simulations the values of γ and ε were chosen so as to ensure $0 \leq \sigma \leq 1$ for all i 's.

We numerically iterated the game on several networks, including the three shown in Figs. 1 (a), (b) and (c) for a number of time-steps and for each node i we monitored $\langle S_i \rangle$ the fraction of times a node spends in the cooperator state. For each run, the game was iterated until a state was reached in which the number of cooperators and defectors stabilized. Figures 1(d), (e) and (f) show $\langle S_i \rangle$, the fraction of times that each node spends in the cooperator state for each one of the nodes of the networks in Fig. 1(a), (b) and (c), respectively.

We now write a set of equations to describe the evolution of the model presented in Eqs. (1) and (2). Since in each time step a randomly chosen node out of the N players is selected to update its strategy, we can write,

$$S_i^{t+1} = \begin{cases} S_i^t & \text{with probability } \frac{N-1}{N} \\ 1 & \text{with probability } \frac{1}{N} \sigma(x_i) \\ 0 & \text{with probability } \frac{1}{N} (1 - \sigma(x_i)) \end{cases} \quad (4)$$

From this equation, we can compute the expected value of S_i at time $t + 1$,

$$\langle S_i \rangle^{t+1} = \frac{N-1}{N} \langle S_i \rangle^t + \frac{1}{N} \langle \sigma(x_i) \rangle, \quad (5)$$

where the symbol $\langle \dots \rangle$ indicates an average over several realizations. By using $\langle \sigma(x_i) \rangle = \sigma(\langle x_i \rangle)$, Eq. (5) becomes,

$$\langle S_i \rangle^{t+1} - \langle S_i \rangle^t = -\frac{1}{N} (\langle S_i \rangle^t - \sigma(\langle x_i \rangle)) \quad (6)$$

The quantity $\langle x_i \rangle = (2 \langle F_{Ci} \rangle - \langle F_i \rangle)$ and from Eqs. (1) and (3) we see that

$$\langle F_i \rangle = \sum_{j=1}^N A_{ij} \langle f_j \rangle = \sum_{j=1}^N A_{ij} [1 - \omega + \omega \langle \xi_j \rangle] \quad (7)$$

and

$$\langle F_{Ci} \rangle = \sum_{j=1}^N A_{ij} \langle S_j f_j \rangle = \sum_{j=1}^N A_{ij} \langle S_j \rangle \langle f_j \rangle = \sum_{j=1}^N A_{ij} \langle S_j \rangle [1 - \omega + \omega \langle \xi_j \rangle] \quad (8)$$

where in order to obtain (8) we have made use of the assumption that S_j and f_j are statistically independent quantities. The assumption of statistical independence is reasonable if the network has few short loops and low average degree, see e.g. [19], [20]. Our numerical results show consistency of the statistical independence assumption.

In vector form, Eq. (6) becomes

$$\langle \mathbf{S} \rangle^{t+1} - \langle \mathbf{S} \rangle^t = -\frac{1}{N} (\langle \mathbf{S} \rangle^t - \sigma(\langle \mathbf{x} \rangle)) \quad (9)$$

where the vectors $\langle \mathbf{x} \rangle = \langle \mathbf{F}_C \rangle - \langle \mathbf{F}_D \rangle = 2 \langle \mathbf{F}_C \rangle - \langle \mathbf{F} \rangle$, $\mathbf{S} = [S_1, S_2, \dots, S_N]$, $\mathbf{F} = [F_1, F_2, \dots, F_N]$ and $\mathbf{F}_C = [F_{C1}, F_{C2}, \dots, F_{CN}]$. From Eq. 9 we see that at steady state, $\langle \mathbf{S} \rangle = \sigma(\langle \mathbf{x} \rangle)$.

Now, $\sigma(\langle \mathbf{x} \rangle) = \sigma(2 \langle \mathbf{F}_C \rangle - \langle \mathbf{F} \rangle) = 2\gamma \langle \mathbf{F}_C \rangle - \gamma \langle \mathbf{F} \rangle + \varepsilon$. We write the payoff vector, $\boldsymbol{\xi} = b\mathbf{A}\mathbf{S} - c\boldsymbol{\Omega}\mathbf{S} = (b\mathbf{A} - c\boldsymbol{\Omega})\mathbf{S}$, where $\boldsymbol{\Omega}$ is a diagonal matrix such that $\Omega_{ii} = \sum_j^N A_{ij}$. Then from Eqs. (7) and (8) we write an expression for $\langle \mathbf{F} \rangle$ and $\langle \mathbf{F}_C \rangle$ in vector form: $\langle \mathbf{F} \rangle = \mathbf{A} [1 - \omega + \omega (b\mathbf{A} - c\boldsymbol{\Omega}) \langle \mathbf{S} \rangle]$ and $\langle \mathbf{F}_C \rangle = \mathbf{A} [\langle \mathbf{S} \rangle \circ (1 - \omega + \omega (b\mathbf{A} - c\boldsymbol{\Omega}) \langle \mathbf{S} \rangle)]$, where, the symbol " \circ " represents the Hadamard Product. We rewrite Eq. (9) as

$$\begin{aligned} \langle \mathbf{S} \rangle^{t+1} &= \frac{(N-1)}{N} \langle \mathbf{S} \rangle^t + \frac{\gamma}{N} [2\mathbf{A} (\langle \mathbf{S} \rangle^t \circ (1 - \omega + \omega (b\mathbf{A} - c\boldsymbol{\Omega}) \langle \mathbf{S} \rangle^t)) \\ &\quad - \mathbf{A} (1 - \omega + \omega (b\mathbf{A} - c\boldsymbol{\Omega}) \langle \mathbf{S} \rangle^t)] + \frac{\varepsilon}{N} \end{aligned} \quad (10)$$

2.1.1 Equivariance

We now focus on the effects of the network symmetries on the dynamics. Our goal is to prove that Eq. (10) is equivariant under permutations of the network nodes that are in the automorphism group of A . We look at Eq. (10) and consider symmetries (Π) of A , that is, Π is a permutation matrix such that $\Pi A = A \Pi$. Let's assume $\langle \mathbf{S} \rangle^{t+1} = G_1(\langle \mathbf{S} \rangle^t)$ and our goal is to prove that $\Pi \langle \mathbf{S} \rangle^{t+1} = G_1(\Pi \langle \mathbf{S} \rangle^t)$.

Applying the permutation matrix Π to $\langle \mathbf{S} \rangle^{t+1}$. Then,

$$\begin{aligned} \Pi \langle \mathbf{S}^{t+1} \rangle &= \frac{(N-1)}{N} \Pi \langle \mathbf{S} \rangle^t + \frac{\gamma}{N} [2\Pi A (\langle \mathbf{S} \rangle^t \circ (1 - \omega + \omega(bA - c\Omega) \langle \mathbf{S} \rangle^t)) \\ &\quad - \Pi A (1 - \omega + \omega(bA - c\Omega) \langle \mathbf{S} \rangle^t)] + \frac{\varepsilon}{N} \\ &= \frac{(N-1)}{N} \Pi \langle \mathbf{S} \rangle^t + \frac{\gamma}{N} [2A \Pi (\langle \mathbf{S} \rangle^t \circ (1 - \omega + \omega(bA - c\Omega) \langle \mathbf{S} \rangle^t)) \\ &\quad - A \Pi (1 - \omega + \omega(bA - c\Omega) \langle \mathbf{S} \rangle^t)] + \frac{\varepsilon}{N} \end{aligned}$$

We note that nodes that are symmetric to each other also have the same degree. Thus from the definition of the matrix Ω it follows that $\Pi \Omega = \Omega \Pi$. Therefore,

$$\begin{aligned} \Pi \langle \mathbf{S}^{t+1} \rangle &= \frac{(N-1)}{N} \Pi \langle \mathbf{S} \rangle^t + \frac{\gamma}{N} [2A (\Pi \langle \mathbf{S} \rangle^t \circ (1 - \omega + \omega(bA - c\Omega) \Pi \langle \mathbf{S} \rangle^t)) \\ &\quad - A (1 - \omega + \omega(bA - c\Omega) \Pi \langle \mathbf{S} \rangle^t)] + \frac{\varepsilon}{N} \\ &= G_1(\Pi \langle \mathbf{S} \rangle^t) \end{aligned}$$

We now attempt to estimate the values attained by the nodes in each cluster. We note that at steady state Eq. (9) can be solved iteratively in the unknown quantities $\langle S \rangle_i$, $i = 1, 2, \dots, N$. This is shown in Fig. 3(a) where $\langle S \rangle_i$ obtained by the iterative solution of Eq. (9) at steady state is plotted versus the value of $\langle S \rangle_i$ obtained from the numerical simulation of the game averaged over a number of realizations. Colors are consistent with Fig. 1(a).

The obtained numerical steady state solution for Eqs. (9) showed that nodes in the same clusters converged on the same values as the contraction mapping was iterated. Mismatches between the theory and the simulations are due to the simplifying assumptions we had to introduce in order to derive the equations for this model.

2.2 Network Traffic Model

In the network traffic model, packets are originated at source nodes, get routed through a sequence of intermediate nodes, until they reach the destination nodes and get removed from the network. We consider a simplified version of the network traffic model studied in [25, 4, 6, 7, 24, 8, 13, 15, 16]. In this model at each time the network evolution is characterized by the following sequence of steps:

1. Each node produces a *data packet* at a given generation rate.
2. Each packet that is generated is assigned a destination, which is a randomly chosen node in the network.
3. Each node has a temporary memory (a *queue*) in which packets are stored. When a node receives a packet it is placed at the bottom of its queue.
4. For each node that has at least one packet in its queue, the packet at the top of the queue is routed to one of its neighboring nodes.
5. The routing of packets depends on the queue length of the neighboring nodes. In what follows we make the assumption that the probability that a packet is routed to a certain node is inversely proportional to the node's queue length. If two or more neighboring nodes are equally preferable for routing then a node is chosen randomly with equal probability.
6. If a packet reaches its target, it is removed from the queue of the destination node.

We call q_i^t the number of packets in the queue of node i at time t and assume $q_i^t \neq 0$. Then at time $t + 1$ the probability that node i sends one packet to node j is equal to,

$$\mathcal{P}_{ji}^{t+1} = \frac{A_{ji} \frac{1}{q_j^t}}{\sum_{\ell} A_{\ell i} \frac{1}{q_{\ell}^t}}, \quad (11)$$

which indicates a lower probability of forwarding packets to nodes with a large queue.

We define the packet generation rate to be λ and the packet delivery rate to be μ_j . Even when the packet generation rate λ is the same for all nodes, the computed packet delivery rate μ_j may vary from node to node. This is because the packets that are on their way to reach certain destinations spend more time in the queues of the intermediary nodes than others, which decreases the effective delivery rate of those destinations.

Then, at time $t + 1$ the queue length of node j will be equal to,

$$q_j^{t+1} = q_j^t + \sum_k A_{jk} \mathcal{P}_{jk}^t + \lambda - \mu_j - \Psi_j, \quad (12)$$

where Ψ_j is the packet routing rate (the average numbers of packets routed by node j in a time step). In the congested state (i.e., for large enough λ), $\Psi_j = 1$ for all j 's; then, by taking into account that the entries of the matrix A are either 0 or 1, Eq. (12) becomes,

$$q_j^{t+1} - q_j^t = \sum_k \frac{A_{jk}}{q_j^t \sum_{\ell} A_{\ell k} \frac{1}{q_{\ell}^t}} + \lambda - \mu_j - 1 \quad (13)$$

It should be noted that the total number of packets must satisfy the following continuity equation

$$\sum_i q_i^t = \left(\lambda N - \sum_i \mu_i \right) t \quad (14)$$

In the simulation we observed that in the congested state the queue lengths of the network nodes grow approximately linearly over time. Based on this observation, we introduce the assumption that, the queue length of node j can be written as $q_j^t \simeq \alpha_j t$, where α_j is the rate of growth of the queue length (*queue angle*) at node j . Then we can write,

$$q_j^{t+1} - q_j^t = \alpha_j = \sum_k \frac{A_{jk}}{\alpha_j t \sum_{\ell} A_{\ell k} \frac{1}{\alpha_{\ell} t}} + \lambda - \mu_j - 1 \quad (15)$$

$$\alpha_j^2 = \sum_k \frac{A_{jk}}{\sum_{\ell} A_{\ell k} \frac{1}{\alpha_{\ell}}} + \alpha_j (\lambda - \mu_j - 1) \quad (16)$$

Moreover, Eq. (14) can be rewritten,

$$\sum_i \alpha_i = \lambda N - \sum_i \mu_i \quad (17)$$

Note that this equation relates the total packet delivery rate $\sum_i \mu_i$ with the total rate of growth of the queue length $\sum_i \alpha_i$. By introducing the quantities $\tilde{\alpha}_i = \frac{1}{\alpha_i}$, we obtain,

$$\alpha_j^2 - \alpha_j (\lambda - \mu_j - 1) = \sum_k \frac{A_{jk}}{\sum_{\ell} A_{\ell k} \tilde{\alpha}_{\ell}} \quad (18)$$

The above equation can be re-written as,

$$\alpha_j (\alpha_j - \lambda + \mu_j + 1) = \sum_k \frac{A_{jk}}{\tilde{\alpha}_k} \quad (19)$$

where, the vector $\hat{\alpha} = A^T \tilde{\alpha}$. In vector form we can write $\mathbf{Q}^t = \alpha t$, where $\mathbf{Q} = \{q_1, q_2, \dots, q_N\}$ and $\alpha = \{\alpha_1, \alpha_2, \dots, \alpha_N\}$. In order to quantify the individual delivery rates μ_j , we have compared different centrality measures (normalized) i.e. degree, eigenvector, Katz, and Page rank where we found the best measures was provided by the degree. Hence, by also using Eq. (17) we obtain the following approximate relation, $\mu_j = \hat{\mu}_j \sum \mu_i = \hat{\mu}_j (\lambda N - \sum \alpha_i) = (d_j / \sum d_i) (\lambda N - \sum \alpha_i)$ where $\hat{\mu}_j$ is the normalized delivery rate at node j and d_i is the degree of node i . Then we rewrite eq. (19) as

$$\alpha_j \left[\alpha_j - \lambda + \frac{d_j}{\sum_i^N d_i} \left(\lambda N - \sum_i^N \alpha_i \right) + 1 \right] = \sum_k^N \frac{A_{jk}}{\tilde{\alpha}_k} \quad (20)$$

By using a contraction mapping Eq. (20) can be solved iteratively in the unknown quantities α_j , that is, in the rates of growth of the queues at different nodes.

In all our experiments, we set the generation rate to be equal to 0.84. That means in average 84% of nodes produce a packet at each time step, which always generated a congested state. Figures 1 (g), (h) and (i) show the queue angle of each node after a million of time steps for the networks in Figs. 1 (a), (b) and (c), respectively. For these networks, the nodes in the same clusters (as determined by the symmetry analysis) display similar queue lengths and also delivery rates. Note that nodes in the same cluster have the same degree (as well as in general, the same centrality measures).

2.2.1 Equivariance

We can rewrite Eq. (13) in vector form,

$$\mathbf{Q}^{t+1} = \mathbf{Q}^t + A (1 \circ^{-1} (A (1 \circ^{-1} \mathbf{Q}^t))) \circ (1 \circ^{-1} \mathbf{Q}^t) + \lambda - \mu - 1 \quad (21)$$

Where, the symbol " $1 \circ^{-1}$ " represents the Hadamard division, i.e., multiplication with the inverse elements of the matrix or vector.

As for the case of the evolutionary game theory dynamics presented in Sec. 2.2.1, assume that Π is a permutation of A . Considering $\mathbf{Q}^{t+1} = G_2(\mathbf{Q}^t)$ we want to show that $\Pi \mathbf{Q}^{t+1} = G_2(\Pi \mathbf{Q}^t)$, We will now try to prove $\Pi \mathbf{Q}^{t+1} = G_2(\Pi \mathbf{Q}^t)$ from Eq. (13) without using the ansatz $q_j^t = \alpha_j^t t$.

We pre-multiply both sides of Eq. (21) by Π and obtain,

$$\begin{aligned} \Pi \mathbf{Q}^{t+1} &= \Pi \mathbf{Q}^t + \Pi A (1 \circ^{-1} (A (1 \circ^{-1} \mathbf{Q}^t))) \circ \Pi (1 \circ^{-1} \mathbf{Q}^t) + \lambda - \mu - 1 \\ &= \Pi \mathbf{Q}^t + A (1 \circ^{-1} (\Pi A (1 \circ^{-1} \mathbf{Q}^t))) \circ (1 \circ^{-1} \Pi \mathbf{Q}^t) + \lambda - \mu - 1 \\ &= \Pi \mathbf{Q}^t + A (1 \circ^{-1} (A (1 \circ^{-1} \Pi \mathbf{Q}^t))) \circ (1 \circ^{-1} \Pi \mathbf{Q}^t) + \lambda - \mu - 1 \\ &= G_2(\Pi \mathbf{Q}^t) \end{aligned}$$

Another way to prove the same result is by using our ansatz $q_j^t = \alpha_j^t t$, which holds for the congested state. Then it follows immediately that $\Pi \alpha = \alpha$ and that $\Pi \mathbf{Q}^{t+1} = G_2(\Pi \mathbf{Q}^t)$.

Figure 3 (b) shows a comparison between the numerical solution for the steady state of Eqs. (20) and full simulation of the network traffic model. Overall, the figure shows good agreement between the analytic and simulation results.

2.3 Biological Excitable Systems

Finally, we consider a network of coupled excitable systems [9]. Each one of these systems can be in either one of three states: quiescent, excited, and refractory. Nodes that are excited can excite neighboring nodes that are in the quiescent state with a certain probability. The Kinouchi and Copelli model [9] has been used to reproduce the activity of networks of coupled biological excitable systems [37, 18, 38]. Each node i in the network is an excitable element and can be in one of $(m + 1)$ states: $\kappa_i = 0$ is the resting state, $\kappa_i = 1$ corresponds to the excited state and the remaining $\kappa_i = 2, \dots, m$ are refractory states, namely states in which an excitable element is unable to receive or respond to an excitation. In each time-step an element (node) that is in resting state can become excited (i.e. transition from $\kappa_i = 0$ to $\kappa_i = 1$) in two ways: either through an external excitation described by a Poisson process with probability η or with a probability A_{ij} for each neighbor j that was in the excited state in the previous

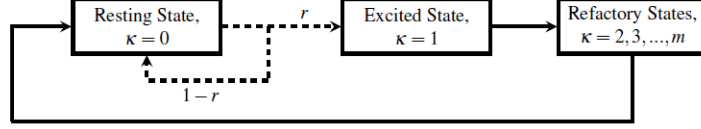


Figure 2: Schematic representation of the Kinouchi-Copelli Model. The dashed lines represent probabilistic transition (from the resting state there's a probability r of transitioning into the excited state and a probability $(1 - r)$ of remaining in the resting state) and solid lines represent deterministic transitions.

time-step. Nodes in the excited and refractory state will transition deterministically into the next refractory state, if available, otherwise return to the resting state (Fig. 2).

The topology of the network is also described by the adjacency matrix $A = \{A_{ij}\}$, where we set $A_{ij} = A_{ji}$ to be equal to $0.5/K$ if node j can excite node i , otherwise $A_{ij} = 0$ and $K = N^{-1} \sum_{i,j} A_{ij}$ is the average node degree of the network. A node that is in the excited or refractory state will deterministically transition into the next refractory state, until $\kappa_i = m$ after which it will transition again into the resting state $\kappa_i = 0$.

Using the analysis developed in Ref. [18] by Larremore *et al.*, in particular Eqs. (9) and (10) from [18], we can write

$$p_i^{t+1} = \left(1 - \sum_{k=1}^m p_i^{t+1-k}\right) \left(\eta + (1 - \eta) \left[1 - \prod_j^N (1 - A_{ij} p_j^t)\right]\right), \quad (22)$$

where p_i^t represents the probability that node i is excited at time t , m is the number of refractory states (i.e. $\kappa = 0, 1, 2, \dots, m$) and η is the probability that a node is excited by an external stimulation. To understand Eq. (22), first note that a node can become excited at time $t + 1$ only if it is in the susceptible state at time t , which explains the first term on the right hand side of Eq. (22). The second term on the right hand side of Eq. (22) represents the probability that a node that is susceptible at time t becomes excited, either via an external excitation described by the probability η or if at least one stimulus is received by one of the neighboring nodes (1 minus the probability that no stimulus is received). Note the underlying assumption of statistical independence. For more details, refer to Ref. [19, 20]. Following [18] by assuming that $A_{ij} p_j$ is small we replace $\prod_j^N (1 - A_{ij} p_j^t)$ by $\exp(-\sum_j^N A_{ij} p_j^t)$ and write,

$$p_i^{t+1} = \left(1 - \sum_{k=1}^m p_i^{t+1-k}\right) \left(\eta + (1 - \eta) \left[1 - \exp\left(-\sum_j^N A_{ij} p_j^t\right)\right]\right) \quad (23)$$

and at steady state,

$$p_i = (1 - m_i p_i) \left(\eta + (1 - \eta) \left[1 - \exp\left(-\sum_j^N A_{ij} p_j\right)\right]\right) \quad (24)$$

We numerically simulated the Kinouchi Copelli model on a number of networks, including the three shown in Figs. 1 (a), (b) and (c). We set $m = 6$, $\eta = 0.01$ and record the average time that each node spends in the excited state over a large number of time-steps. Figures 1 (j), (k) and (l) show the average fraction of times a node spends in the excited state after a million of time-steps for all three networks in Figs. 1 (a), (b) and (c). We see that the effect of the network symmetries is apparent for the nodes that are in the same cluster and for all the networks considered.

2.3.1 Equivariance

We also want to analyze the effect of symmetry in the biological excitable system [9], [18]. To this end, we write the vector versions of Eq.(23) and Eq.(24),

$$\mathbf{P}^{t+1} = \left(1 - \sum_{k=1}^m \mathbf{P}^{t+1-k}\right) \circ (\eta + (1 - \eta) [1 - \exp(-A\mathbf{P}^t)]) \quad (25)$$

and for the steady state,

$$\mathbf{P} = (1 - m\mathbf{P}) \circ (\eta + (1 - \eta) [1 - \exp(-A\mathbf{P})]) \quad (26)$$

We look at Eq. (25) and consider symmetries (Π) of A , that is permutation matrices such that $\Pi A = A \Pi$. Again, we assume that Π permutes with $\mathbf{P}^t, \mathbf{P}^{t-1}, \dots, \mathbf{P}^{t-m+1}$ then we want to show that Π also permutes with \mathbf{P}^{t+1} . Lets, $\mathbf{P}^{t+1} = G_3(\mathbf{P}^t)$. For this model our goal is to show $\Pi \mathbf{P}^{t+1} = G_3(\Pi \mathbf{P}^t)$ Let's premultiply both sides of the Eq. (25) by Π and write,

$$\begin{aligned}
\Pi \mathbf{P}^{t+1} &= \Pi \left(\left(1 - \sum_{k=1}^{m_i} \mathbf{P}^{t+1-k} \right) \circ (\eta + (1 - \eta) [1 - \exp(-A \mathbf{P}^t)]) \right) \\
&= \Pi \left(1 - \sum_{k=1}^{m_i} \mathbf{P}^{t+1-k} \right) \circ \Pi (\eta + (1 - \eta) [1 - \exp(-A \mathbf{P}^t)]) \\
&= \left(1 - \Pi \sum_{k=1}^{m_i} \mathbf{P}^{t+1-k} \right) \circ (\eta + (1 - \eta) [1 - \exp(-\Pi A \mathbf{P}^t)]) \\
&= \left(1 - \sum_{k=1}^{m_i} \Pi \mathbf{P}^{t+1-k} \right) \circ (\eta + (1 - \eta) [1 - \exp(-A \Pi \mathbf{P}^t)]) \\
&= G_3(\Pi \mathbf{P}^t)
\end{aligned}$$

We note that Eq. (26) can be iteratively solved in the unknown quantities P_1, P_2, \dots, P_N . This is shown in Fig. 3(c) where we plotted the average status of a node from iteration of Eq. (26) versus the average time that the node is found in the excited state from the full simulation of the Kinouchi and Copelli model [9]. Mismatches between the theory and the simulations are due to the simplifying assumptions we had to introduce in order to derive the equations for this model.

For each one of the dynamical models considered, we have performed an analysis to: (i) predict the emergence of clusters when the dynamics is averaged in time and (ii) predict the values attained by the nodes in each cluster. Our main result is that for all the three networks and the three dynamical models, *nodes that belong to the same cluster show the same time-averaged dynamics*. This is illustrated in detail in Fig. 1 (d)-(l). While this observation holds irrespective of the particular network and type of dynamics, the particular time-averaged value attained by the nodes in the same cluster is network and model specific. Note that in the figure nodes are ordered by their degree (which is the label on the abscissa-axis). For example, for the game theory model, we observe that the nodes in the same cluster approximately show the same frequency of being a cooperator (or defector) but that does not necessarily correlate with the degree. Here we see that the symmetries in the network topology can predict dynamics better than the nodes' degrees.

3 Quotient Graph Reduction

As mentioned in the introduction, symmetries are common features of biological networks, technological networks, social networks etc. MacArthur *et al.* [46] have analyzed datasets of large complex networks and have found that these present large numbers of symmetries, see Supplementary Information Sec. S1. Intensive research in social sciences, biology, engineering, and physics uses numerical simulations of large complex networks to understand and predict their dynamical behavior (e.g., in a given network, the critical value of the infection rate above which an epidemics occurs), in order to better characterize and control real-world phenomena.

Our results in Sec. 2 point out that nodes that are related by a symmetry operation display the same time-averaged dynamical behavior. This immediately raises the question whether a reduction of the dynamics is possible in which *duplicate nodes* can be omitted, leading to *minimal models* of complex networks, and so to a better exploitation of computational resources in numerical simulations, such as computation time and memory. Related questions have been asked in the literature of complex networks, where nodes have been grouped according to some of their features, most notably the degree [27] and these approaches have been successful at predicting and explaining several network properties, in particular in the case of scale free networks [42]. While these approaches are typically based on mean-field models and thus approximate, here our grouping of nodes is based on the exact concept of a symmetry.

Our ultimate goal is to generate minimal network models that reproduce certain features of the dynamics by using the least possible number of nodes. In the case of synchronization dynamics, we know that a *quotient*

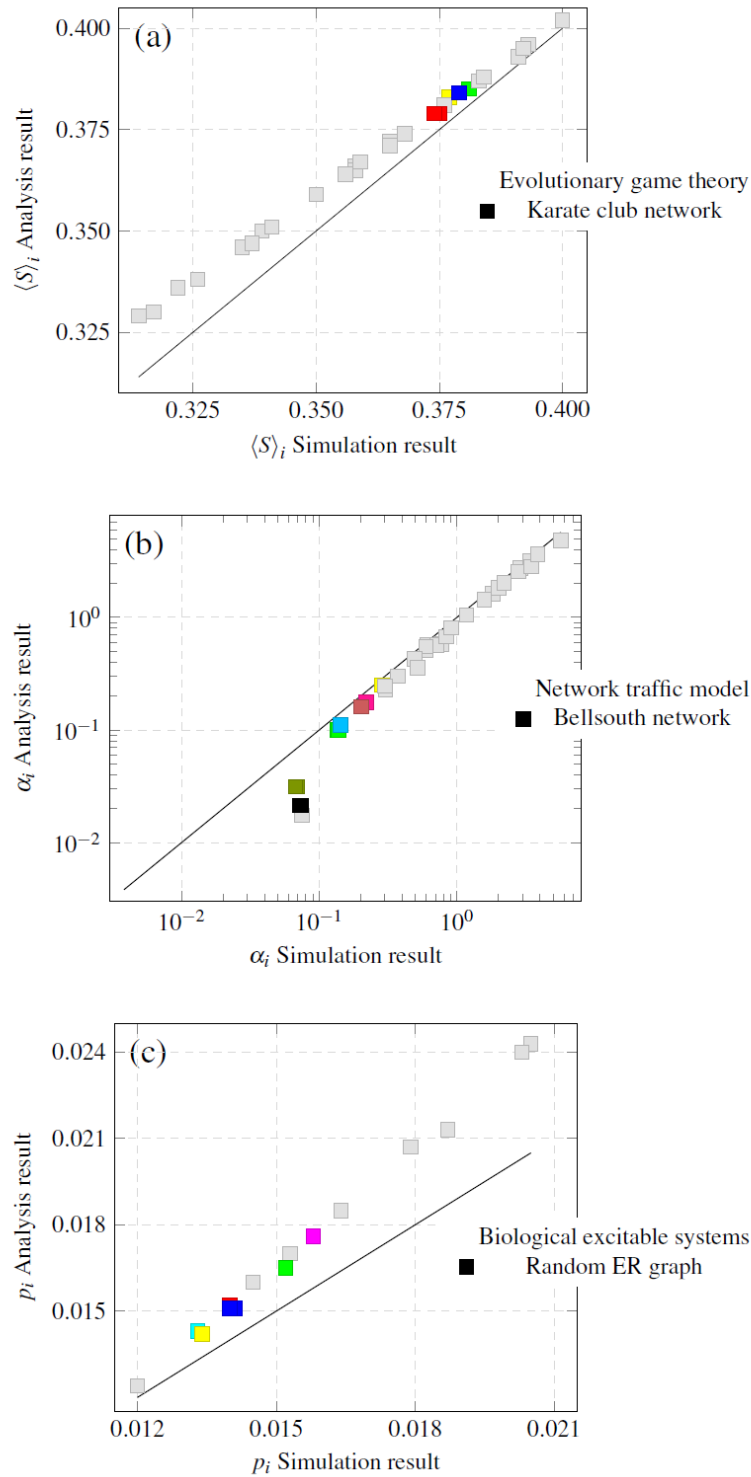


Figure 3: Each plot shows a comparison between the iterative solutions and the full simulation results for the three dynamical scenarios shown in Fig. 1(a, d), (b, h), and (c, l). The following three cases are considered: (a) evolutionary game theory on the Karate club network, (b) network traffic dynamics on the Bellsouth network and (c) spread of excitation in a random network of excitable systems. Points that are colored the same correspond to nodes in the same cluster (coloring is consistent with Fig. 1(a), (b) and (c), except for the gray colored nodes, each of which is in a cluster by itself).

network reduction is possible, in which the exact cluster-synchronous time-evolution is generated by a minimal number of nodes (i.e., one node for each cluster). However, how to obtain minimal network models for other types of dynamics, remains an open question. To address this issue, here we will briefly review the concept of a *quotient network*.

Under the action of the symmetry group, the set of the network nodes is partitioned into C disjoint structural equivalence classes called the group *orbits*, $\mathcal{O}_1, \mathcal{O}_2, \dots, \mathcal{O}_C$, such that $\bigcup_{\ell=1}^C |\mathcal{O}_\ell^i| = N$ and $\mathcal{O}_\ell^i \cap \mathcal{O}_\ell^j = \emptyset$, where $i, j = 1, 2, \dots, C, j \neq i$.

Then we can define a $C \times C$ matrix \hat{A} corresponding to the quotient network such that for each pair of sets $(\mathcal{O}^v, \mathcal{O}^u)$,

$$\hat{A}_{uv} = \sum_{j \in \mathcal{O}^v} A_{ij}, \quad (27)$$

for any $i \in \mathcal{O}^u$ (i.e., independent of $i \in \mathcal{O}^u$), and for $u, v = 1, 2, \dots, C$.

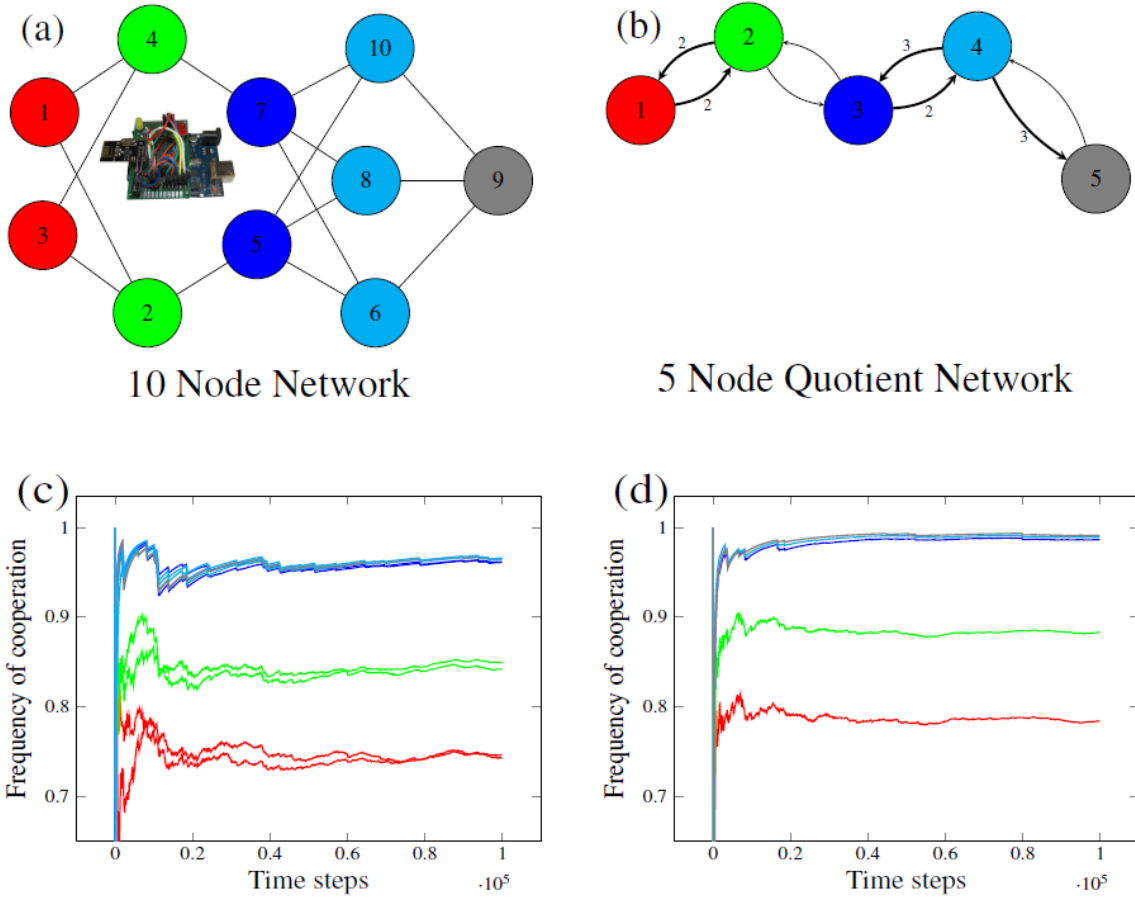


Figure 4: (a) A 10 node network and (b) its 5 node quotient reduction. Inset of (a) shows one arduino board with radio transmitter, which we used in our experiments. Plots (c) and (d) are experimental time traces showing the running average for the fraction of times each node spends in the cooperator state for the full network in (a) and the quotient network in (b), respectively. Colors in (c) and (d) are consistent with (a) and (b).

In Fig. 4(a) we show a randomly generated network of 10 nodes and in Fig. 4(b) its quotient graph reduction. We see that all the nodes in the same cluster (these are colored the same in the figure on the left), map to only one node of the quotient network (on the right) and the color identifies the reduced node. Note that the quotient network may be directed even if the original full network is undirected. It is also possible that nodes of the quotient network form self connections, which represent connections between nodes belonging to the same cluster in the original graph.

In general, the mathematical equations we have derived in Sec. 2 for all the three models can be projected onto the corresponding quotient network equations (see the Supplementary Information Sec. S1 for an example). However, obtaining an equivalent model that can be simulated on the quotient network and reproduce the original full network dynamics may require a particular adaptation of the model, which is model specific.

We show that the quotient graph can be conveniently exploited in simulations involving large networks to reduce computation time and memory. These simulations may be used to model various type of dynamics, including epidemics, congestion, emergence of cooperation, as discussed in Sec. 2, just to mention a few examples. In order to demonstrate this point we consider the evolutionary game theory model presented in Sec. 2 and for a number of networks, we study how well the corresponding quotient graphs can approximate the evolutionary dynamics of the original full network. In what follows we describe evolution of the Prisoner's Dilemma dynamics, as described in Sec. 2, on the quotient network. We indicate with $\hat{S}_j = \{0, 1\}$ the strategy of node j of the quotient network, where 0 represents defection and 1 represents cooperation. At each iteration of the game, the payoff received by quotient node i from its neighboring nodes is equal to $\hat{\xi}_i = \sum_j \hat{A}_{ij} (b\hat{S}_j - c\hat{S}_i)$. Note that this expression for the payoff differs from that for the full network in Eq. (1) as the mapping of nodes from the full network to the quotient network preserves the indegree of the nodes, but not the outdegree. Moreover, the fitness of quotient node i is equal to $\hat{f}_i = 1 - \omega + \omega\hat{\xi}_i$. Similarly we write the expressions,

$$\begin{aligned}\hat{F}_i &= \sum_j \hat{A}_{ij} \hat{f}_j \\ \hat{F}_{Ci} &= \sum_j \hat{A}_{ij} \hat{S}_j (1 - \omega) + \omega \sum_j \hat{A}_{ij} \hat{S}_j \hat{\xi}_j \\ \hat{F}_{Di} &= \sum_j \hat{A}_{ij} (1 - \hat{S}_j) (1 - \omega) + \omega \sum_j \hat{A}_{ij} (1 - \hat{S}_j) \hat{\xi}_j\end{aligned}\tag{28}$$

where \hat{F}_i , \hat{F}_{Ci} and \hat{F}_{Di} are the total fitness, the fitness of the neighboring cooperators, and the fitness of the neighboring defectors of a quotient node i , respectively. We set the same cost c and benefit b as for the full network. At each time step, a node of the quotient network is selected with probability proportional to the cardinality of its orbit set and replaced by a new offspring. This new node becomes a cooperator with a probability $\sigma(\hat{F}_{Ci} - \hat{F}_{Di})$, where σ is the function defined in Sec. 2.

We expect that the time averages $\langle \hat{\xi}_f \rangle \approx \langle \hat{\xi}_q \rangle$, $\langle F_{Cf} \rangle \approx \langle \hat{F}_{Cq} \rangle$ and $\langle F_{Df} \rangle \approx \langle \hat{F}_{Dq} \rangle$, where node f of the full network maps to node q of the quotient network (for nodes of the full network that are in the same cluster, we know that the time averages are the same from the analysis in Sec. 2). Moreover, the time-averaged strategy for a node of the quotient network $\langle \hat{S}_q \rangle$ is the same as the time-averaged strategy for the corresponding node of the full network, $\langle S_f \rangle$. Figure 5 compares the simulation results for the Bellsouth network (squares) and its quotient reduction (diamonds). As can be seen, we find very good agreement between the full and quotient network time-averaged dynamics. This indicates that, if we are interested in the time-averaged behavior, we can equivalently perform a simulation on the full network or on the reduced quotient network.

In order to test the robustness of our results in a real setting, we have built an experimental network of coupled agents iteratively playing the Prisoner's Dilemma. This network is composed of 10 wirelessly coupled transceiver modules as shown in Fig. 4a using nRF24L01 2.4 GHz RF transceivers on Arduino boards. The transceiver modules act as the nodes of the network. All the transceiver modules have unique addresses, i.e., communication is one to one. To construct this network, communication links of each module are restricted as per the topology of the network, i.e., only the connected modules can communicate and share information with each other. For example, radio module 7 in Fig. 4a can only communicate with modules 4, 6, 8, and 10. This experimental realization is subject to practical limitations that are hard to reproduce in simulation. In particular, in our experimental setting these limitations are mainly imposed by the reliability of the radio communication between the individual units. We have also built an experimental version of the quotient network in Fig. 4b. The experimental time traces for the networks in Fig. 4a and b when the game is played are shown in Fig. 4c and d, respectively. We see that: i) nodes of the full network that are in the same cluster attain the same frequency of cooperation as the game is iterated and ii) for large time the quotient network well predicts the full network experimental dynamics.

Since the quotient graphs have in general fewer nodes than the full graphs, they can be advantageous in terms of both memory and time needed in simulation. The size of the adjacency matrix reduces from $N \times N$ to $C \times C$ and the number of nonzero elements of the matrix decreases from NK_{av} to roughly $\sqrt{NC}K_{av}$, where K_{av} is the average node degree of the full network. We define the reduction coefficient $\rho_g = C/N$. A smaller value of the

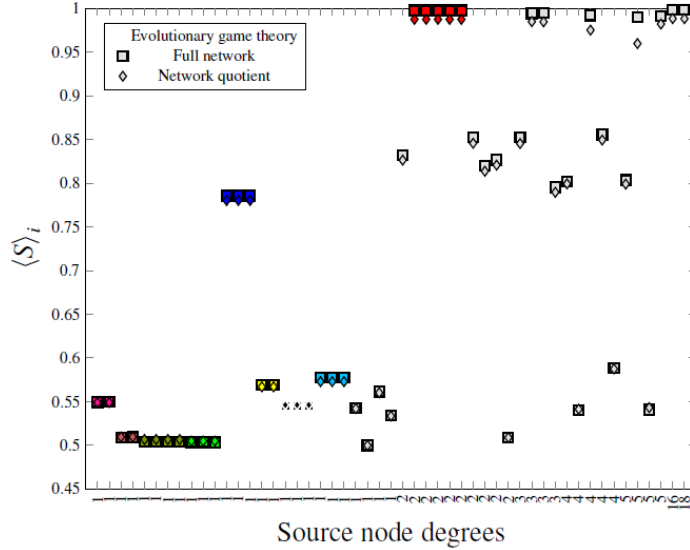


Figure 5: Comparison between simulation results of the evolutionary game on the Bellsouth network in Fig. 1(b) and its quotient version. The diamond marks correspond to simulation on the full network and the square marks correspond to the simulation on the quotient network. Points that are colored the same correspond to nodes in the same cluster (coloring is consistent with Fig. 1(a) and (b), except for the gray colored nodes, each of which is in a cluster by itself).

ratio ρ_g indicates higher reduction of the number of nodes in the quotient graph with respect to the original graph. Note that a critical aspect of simulation of large real networks is the limitation of software memory allocation. We computed the CPU time required by a single iteration of the prisoner’s dilemma dynamics for several networks and their quotients. Fig. 6(a) and Table S2 in the Supplementary Information show the CPU time ratio $\rho_t = t_q/t_f$, where t_f and t_q are the CPU time for an iteration of full and quotient network, respectively.

For both the full network and the quotient network we also computed the simulation convergence time, which we measured as follows. We randomly picked an initial condition for each node of the quotient network and assigned the same initial condition to all the nodes in the corresponding cluster of the full network. At each time step, we computed the running average for the fraction of times a node spent in the cooperation state. For each node we measured its individual convergence time, i.e., the time after which the running average remained steadily in a $[-\delta, +\delta]$ interval of the final state. The convergence time of the network was taken to be the largest of the convergence times of the nodes. Fig. 6(b) and Table S2 in the Supplementary Information show the convergence time ratio $\rho_c = \tau_q/\tau_f$, where τ_f and τ_q are the convergence times for the full and the quotient network, respectively.

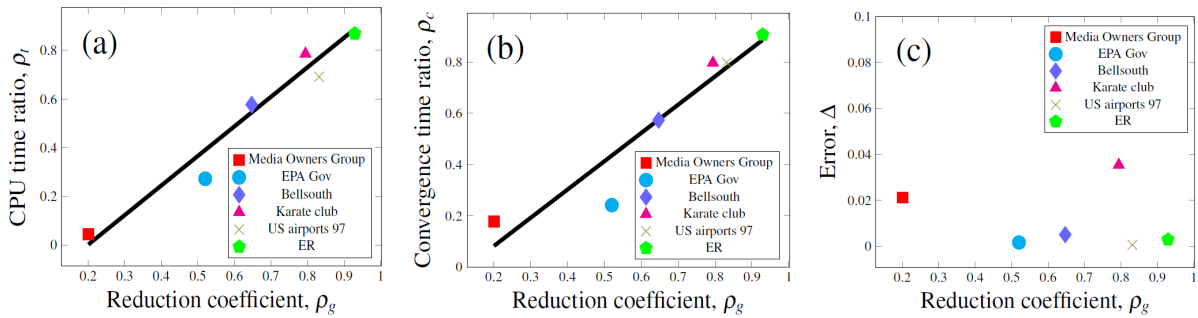


Figure 6: (a) CPU time ratio (b) Convergence time ratio (c) Error between the full and quotient network time-averaged dynamics.

We note that simulating the dynamics on the quotient graph, rather than on the original network, can reduce the computational effort, while producing approximately the same time-averaged dynamics. In Fig. 6(c) and Table S2 in the Supplementary Information we show the accuracy parameter Δ , defined as the normalized average difference of the time-averaged frequency of cooperation between the full and the quotient networks,

$$\Delta = \frac{1}{N} \sum_i^N \frac{|\langle S \rangle_i - \langle \hat{S} \rangle_i|}{S_i}, \quad (29)$$

where $\langle S \rangle_i$ and $\langle \hat{S} \rangle_i$ are the time-averaged frequency of cooperation of node i and its corresponding node in the quotient network, respectively.

Figure 6 shows that as the reduction coefficient is lowered, the CPU time ratio ρ_t and the convergence time ratio ρ_c decrease in a linear fashion but the normalized error parameter Δ is roughly independent of ρ_g . It is important to look at the y -axes of the plots in Figs. 6(a), (b) and (c). For example, for a strong reduction coefficient $\rho_g \simeq 0.2$, corresponding to the Media Owners Group network, the CPU time is lowered by roughly 95% but the normalized error Δ only increases by approximately 2%.

4 Experimental realization

In order to test the robustness of our results in a real setting, we have built an experimental network of coupled agents that iteratively play the Prisoner’s Dilemma. This network is composed of 10 coupled wireless transceiver modules as shown in Fig. 7(b) using nRF24L01 2.4 GHz RF transceivers on Arduino boards. The transceiver modules act as the nodes of the network. All the transceivers modules have unique addresses and the serial communication is one to one. To construct this network, communication links of each module are restricted as per the topology of the network, i.e., only the connected modules can communicate and share information with each other. For example, radio module 8 only can communicate with modules 5, 7 and 9. For this network communication is bidirectional.

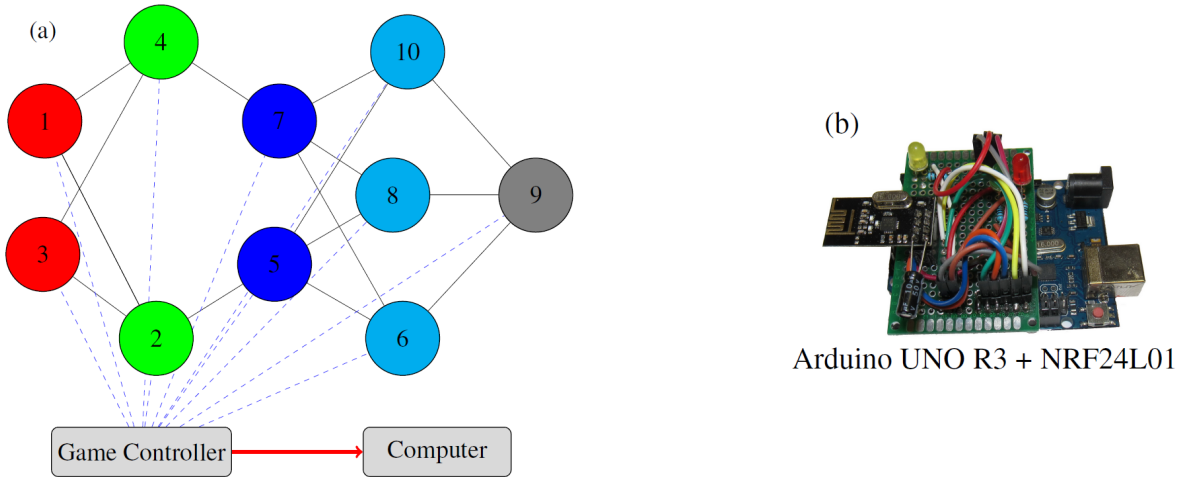


Figure 7: (a) Schematic of the experiment (b) A physical node of the network

This experimental realization is subject to experimental limitations that cannot be captured in simulation. In particular, in our experimental setting, these limitations are mainly imposed by the reliability of the radio communication between the individual units. For every signal sent from a sender to a receiver, an acknowledgement signal is sent back from the receiver to the sender, in order for the game to proceed.

In our practical implementation, another wireless transceiver module, the *game controller*, is added to the network. This game controller is not part of the network topology but connected (blue dashed links in the figure) to all the agents. The controller assigns tasks in a sequence to all nodes. When a task is completed, nodes send an accomplishment message back to the controller. While the controller tells the other nodes what to do and when to

do it, it does not affect the exchange of information between the nodes, which is decentralized. In particular, the controller does not transmit any information related to the game (strategies and payoffs of the nodes). The functions of the controller are the following: (i) it enforces that the other nodes execute activities in a specific sequence, (ii) it randomly selects at each iteration of the game the node whose strategy is updated, (iii) it ensures that at every time only one node is sending a message while the other nodes are in receiving mode, and (iv) after each iteration of the game, the controller sends the network status to a computer, where the data from the experiment is stored.

According to the serial protocol, at every time only one agent can send signals to its neighbors and the receivers cannot receive multiple signals simultaneously. Sometimes the acknowledgment of a signal may not be available for a short period of time for several reasons, for example the signal may not reach the receiver or the receiver receives through the same radio channel multiple signals at the same time from different sources. For this experiment, the code for each agent is written in state/machine fashion so that it can adjust for a temporary break of the communication between two agents with the help of the game controller. If the controller does not receive an accomplishment signal from a certain node in a specified time interval, it will resend the same task message to that same node. This will continue for a fixed number of iterations until a successful task accomplishment message is received. If that does not happen, a new random selection of a node is made and the task is sent to the new node.

5 Conclusions

By applying a symmetry analysis to a network, we have uncovered clusters of nodes that are structurally and functionally equivalent. This becomes apparent when monitoring the time-averaged state of the nodes in a variety of network models (previous work had only focused on the particular case of synchronization dynamics) and is confirmed in an experimental realization of an evolutionary game played on a network, in the presence of noise and communication losses. Thus it appears that the emergence of symmetry clusters in the time-averaged dynamics of networks is a quite general feature. For the case of the evolutionary game, we obtain a reduction technique for exact, yet minimal, simulation of complex networks dynamics, which produces similar dynamical results, while computation requires less time and memory. However, a generalization of this quotient network reduction to other types of dynamics is nontrivial. The reason is that each dynamical model involves a different set of *rules*, which may be difficult to convert into equivalent rules for the quotient network. We hope our work will stimulate further research into reduction techniques that can be applied in a variety of dynamical models.

Acknowledgement. This work was supported by the Office of Naval Research through ONR Award No. N00014-16-1-2637, the National Science Foundation through NSF grant CMMI- 1400193, NSF grant CRISP-1541148, and the Defense Threat Reduction Agency's Basic Research Program under grant No. HDTRA1-13-1-0020. The authors acknowledge help in running the experiment from Robert Morris, Jonathan Ungaro, John Padilla, and Shakeeb Ahmad, all students at the University of New Mexico.

Author contributions. A.B.S. worked on the analysis, numerical simulations, and the experimental setup. F.S. wrote the manuscript. F.S. and L.P. supervised the research.

References

- [1] Arkady Pikovsky, Michael Rosenblum, and Jürgen Kurths. *Synchronization: A Universal Concept in Non-linear Sciences*. Cambridge University Press, 2003.
- [2] Annette F Taylor, Mark R Tinsley, Fang Wang, Zhaoyang Huang, and Kenneth Showalter. Dynamical quorum sensing and synchronization in large populations of chemical oscillators. *Science*, 323(5914):614-617, 2009.
- [3] , Mark R Tinsley, Simbarashe Nkomo, and Kenneth Showalter. Chimera and phase-cluster states in populations of coupled chemical oscillators. *Nature Physics*, 8(9):662-665, 2012.
- [4] K.-I. Goh, B. Kahng, and D. Kim. Packet transport and load distribution in scale-free network models. *Physica A*, 318:72-79, 2003.
- [5] M. G. Rosenblum, A. S. Pikovsky, and J. Kurths. Phase synchronization of chaotic oscillators. *Phys. Rev. Lett.*, 76:1804, 1996.
- [6] R.V. Sole and S.Valverde. Information transfer and phase transition in a model of data traffic. *Physica A*, 289(595), 2001.
- [7] Toru Ohira and Ryusuke Sawatari. Phase transition in a computer network traffic model. *Physical Review E*, 58(1):193, 1998.
- [8] R. Guimerà, A. Díaz-Guilera, F. Vega-Redondo, A. Cabrales, and A. Arenas. Optimal network topologies for local search with congestion. *Phys. Rev. Lett.*, 89(24), 2002.
- [9] Osame Kinouchi and Mauro Copelli. Optimal dynamical range of excitable networks at criticality. *Nature physics*, 2(5):348-351, 2006.
- [10] D. B. Larremore, W. L. Shew, and J. G. Restrepo. Predicting criticality and dynamic range in complex networks: effects of topology. *Phys. Rev. Lett.*, 106:058101, 2011.
- [11] Daniel B Larremore, Woodrow L Shew, Edward Ott, and Juan G Restrepo. Effects of network topology, transmission delays, and refractoriness on the response of coupled excitable systems to a stochastic stimulus. *Chaos: An Interdisciplinary Journal of Nonlinear Science*, 21(2):025117, 2011.
- [12] Louis M Pecora, Francesco Sorrentino, Aaron M Hagerstrom, Thomas E Murphy, and Rajarshi Roy. Cluster synchronization and isolated desynchronization in complex networks with symmetries. *Nature communications*, 5:304-305, 2014.
- [13] David Arrowsmith, Mario di Bernardo, and Francesco Sorrentino. Communication models with distributed transmission rates and buffer sizes. In *Circuits and Systems, 2006. ISCAS 2006. Proceedings. 2006 IEEE International Symposium on*, pages 4-pp. IEEE, 2006.
- [14] Francesco Sorrentino, Louis M Pecora, Aaron M Hagerstrom, Thomas E Murphy, and Rajarshi Roy. Complete characterization of stability of cluster synchronization in complex dynamical networks. *Science Advances* 2, 2015.
- [15] David Arrowsmith, Mario Di Bernardo, and Francesco Sorrentino. Effects of variations of load distribution on network performance. In *Circuits and Systems, 2005. ISCAS 2005. IEEE International Symposium on*, pages 3773-3776. IEEE, 2005.
- [16] Mario di Bernardo and Francesco Sorrentino. Network structural properties, communication models and traffic dynamics. *Nolta*, 2006.
- [17] Hisashi Ohtsuki, Christoph Hauert, Erez Lieberman, and Martin A Nowak. A simple rule for the evolution of cooperation on graphs and social networks. *Nature*, 441(7092):502-505, 2006.
- [18] Daniel B Larremore, Woodrow L Shew, Edward Ott, and Juan G Restrepo. Effects of network topology, transmission delays, and refractoriness on the response of coupled excitable systems to a stochastic stimulus. *Chaos: An Interdisciplinary Journal of Nonlinear Science*, 21(2):025117, 2011.

- [19] Juan G. Restrepo, Edward Ott, and Brian R. Hunt. Weighted percolation on directed networks. *Phys. Rev. Lett.*, 100:058701, Feb 2008.
- [20] Andrew Pomerance, Edward Ott, Michelle Girvan, and Wolfgang Losert. The effect of network topology on the stability of discrete state models of genetic control. *Proceedings of the National Academy of Sciences*, 106(20):8209-8214, 2009.
- [21] SageMath - a free open-source mathematics software. <http://www.sagemath.org/index.html>.
- [22] The internet topology zoo. <http://www.topology-zoo.org/dataset.html>.
- [23] Wayne W Zachary. An information flow model for conflict and fission in small groups. *Journal of anthropological research*, pages 452-473, 1977.
- [24] Y.Moreno, R.Pastor-Satorras, A.Vasquez, and A.Vespignani. Critical load and congestion instabilities in scale-free networks. *cond-mat*, 1(0209474), 2002.
- [25] K.-I. Goh, B. Kahng, and D. Kim. Universal behavior of load distribution in scale-free networks. *Phys. Rev. Lett.*, 87:278701, 2001.
- [26] Simon Knight, Huan X Nguyen, Nick Falkner, Richard Bowden, and Matthew Roughan. The internet topology zoo. *Selected Areas in Communications, IEEE Journal on*, 29(9):1765-1775, 2011.
- [27] Romualdo Pastor-Satorras and Alessandro Vespignani. Epidemic spreading in scale-free networks. *Physical review letters*, 86(14):3200, 2001.
- [28] D. B. Larremore, W. L. Shew, and J. G. Restrepo. Predicting criticality and dynamic range in complex networks: effects of topology. *Phys. Rev. Lett.*, 106:058101, 2011.
- [29] Ben D MacArthur and Rub n J S nchez-Garc a. Spectral characteristics of network redundancy. *Physical Review E*, 80(2):026117, 2009.
- [30] Martin Golubitsky, Ian Stewart, et al. *Singularities and groups in bifurcation theory, volume 2*. Springer Science & Business Media, 2012.
- [31] Martin Golubitsky and Ian Stewart. *The symmetry perspective: from equilibrium to chaos in phase space and physical space, volume 200*. Springer Science & Business Media, 2003.
- [32] Louis M Pecora and Thomas L Carroll. Synchronization in chaotic systems. *Physical review letters*, 64(8):821, 1990.
- [33] Cristopher Moore and Mark EJ Newman. Epidemics and percolation in small-world networks. *Physical Review E*, 61(5):5678, 2000.
- [34] Ayalvadi Ganesh, Laurent Massouli , and Don Towsley. The effect of network topology on the spread of epidemics. In *INFOCOM 2005. 24th Annual Joint Conference of the IEEE Computer and Communications Societies. Proceedings IEEE, volume 2*, pages 1455-1466. IEEE, 2005.
- [35] David JD Earn, Pejman Rohani, Benjamin M Bolker, and Bryan T Grenfell. A simple model for complex dynamical transitions in epidemics. *Science*, 287(5453):667-670, 2000.
- [36] J rgen W Weibull. *Evolutionary game theory*. MIT press, 1997
- [37] Mauro Copelli and Paulo RA Campos. Excitable scale free networks. *The European Physical Journal B*, 56(3):273-278, 2007.
- [38] Lucas S Furtado and Mauro Copelli. Response of electrically coupled spiking neurons: a cellular automaton approach. *Physical Review E*, 73(1):011907, 2006.
- [39] Michelle Girvan and Mark EJ Newman. Community structure in social and biological networks. *Proceedings of the national academy of sciences*, 99(12):7821-7826, 2002.

- [40] Mark EJ Newman. Mixing patterns in networks. *Physical Review E*, 67(2):026126, 2003.
- [41] Mark EJ Newman. Assortative mixing in networks. *Physical review letters*, 89(20):208701, 2002.
- [42] Albert-László Barabási and Réka Albert. Emergence of scaling in random networks. *science*, 286(5439):509-512, 1999.
- [43] Shaolin Tan, Jinhua Lu, Guanrong Chen, and David J Hill. When structure meets function in evolutionary dynamics on complex networks. *Circuits and Systems Magazine, IEEE*, 14(4):36-50, 2014.
- [44] Zhi-Xi Wu and Ying-Hai Wang. Cooperation enhanced by the difference between interaction and learning neighborhoods for evolutionary spatial prisoner's dilemma games. *Physical Review E*, 75(4):041114, 2007.
- [45] Jing Wang, Bin Wu, Xiaojie Chen, and Long Wang. Evolutionary dynamics of public goods games with diverse contributions in finite populations. *Physical Review E*, 81(5):056103, 2010.
- [46] Ben D MacArthur, Rubén J Sánchez-García, and James W Anderson. Symmetry in complex networks. *Discrete Applied Mathematics*, 156(18):3525-3531, 2008.
- [47] Stefano Boccaletti, Vito Latora, Yamir Moreno, Martin Chavez, and D-U Hwang. Complex networks: Structure and dynamics. *Physics reports*, 424(4):175-308, 2006.
- [48] Vincenzo Nicosia, Miguel Valencia, Mario Chavez, Albert Díaz-Guilera, and Vito Latora. Remote synchronization reveals network symmetries and functional modules. *Physical review letters*, 110(17):174102, 2013.
- [49] Igor Belykh, Martin Hasler, Menno Lauret, and Henk Nijmeijer. Synchronization and graph topology. *International Journal of Bifurcation and Chaos*, 15(11):3423-3433, 2005.
- [50] Igor Belykh, Enno de Lange, and Martin Hasler. Synchronization of bursting neurons: What matters in the network topology. *Physical review letters*, 94(18):188101, 2005.
- [51] Igor Belykh and Martin Hasler. Mesoscale and clusters of synchrony in networks of bursting neurons. *Chaos: An Interdisciplinary Journal of Nonlinear Science*, 21(1):016106, 2011.
- [52] Vladimir N Belykh, Igor V Belykh, and Erik Mosekilde. Cluster synchronization modes in an ensemble of coupled chaotic oscillators. *Physical Review E*, 63(3):036216, 2001.